RSC Advances

ROYAL SOCIETY OF CHEMISTRY

www.rsc.org/advances

Journal Name

RSCPublishing

ARTICLE

Self-powered sensor for Hg^{2+} detection based on Hollow-Channel Paper Analytical Devices

Cite this: DOI: 10.1039/x0xx00000x

Received 00th January 2012,
Accepted 00th January 2012

DOI: 10.1039/x0xx00000x

www.rsc.org/

Lina Zhang,[a] Yanhu Wang,[b] Chao Ma,[b] Panpan Wang,[b] and Mei Yan*[b]

In this work, a novel and effective self-powered device was introduced into a microfluidic paper-based analytical device (μ-PAD) with hollow channels to transport fluids for mercury ion (Hg^{2+}) detection. In this device, a mediator-less and compartment-less glucose/O_2 biofuel cell (BFC) device served as the core component where using gold nanoparticles (AuNPs) and platinum nanoparticles functionalized carbon nanotube (Pt/CNT) modified paper electrode as the anodic and cathodic substrate, respectively. For constructing the self-powered Hg^{2+} sensor, an Hg^{2+}-specific oligonucleotide capture aptamer was first immobilized on AuNPs modified anode. In the presence of Hg^{2+}, a AuNPs@glucose dehydrogenase (GDH) labeled signal aptamer was hybridized with the immobilized capture probe through thymine (T)-Hg^{2+}-T interaction. Nicotinamide adenine dinucleotide (NAD^+/NADH) was used as a cofactor in the proposed BFC device, and GDH in the anode could catalyze oxidation of glucose used as fuel to generate gluconolactone, protons and electrons. Meanwhile the Pt/CNT in the cathode showed the direct bioelectrocatalytic toward oxygen reduction reaction (ORR). At optimal conditions, such self-powered sensor could detect Hg^{2+} at picomole level that provided a simple approach to fabricate low-cost and portable power devices on small-size paper for point-of-care testing. In addition, this self-powered sensor could be also used as a power tool for a wide range of potential applications in biotechnology and medicine.

Introduction

Microfluidic paper-based analytical devices (μ-PADs) which are particularly well-adopted as a platform for the development of simple and cost-effective molecular diagnostic assays have been drawn increasing interest since Martinez and co-workers pioneered this field from 2007.[1] To date, various scientific and technical about analytical methods on μ-PADs has been demonstrated.[2] However, some limitations of the slow fluids flow in paper channels were also distinct, such as time-consuming and solvent evaporation which are not beneficial to point-of-care testing. Recently, instead of cellulose network, μ-PADs with hollow channels for fluids transport have been demonstrated.[3] Compared with cellulose networks, the hollow channel μ-PADs possessed the distinguished advantage of easy fabrication, with no pump requirement and rapid fluid flow facilitation appropriate for point-of-care testing.[4]

Environmental contamination with heavy metal ions has created a pressing public health concerning in living systems due to their severe effects on human health and the environment. Consequently, heavy metal ions monitoring in aquatic ecosystems has come to an important issue. As one of the heavy metal ions, mercury ion (Hg^{2+}), widely distributed in air, water, soil, and even food, which is not biodegradable and retained in the ecosystem, is a potent neurotoxin as it can accumulate in the vital organs and tissues binding with sulfur-containing proteins and enzymes, making some important cell functions inactivated that resulted in a variety of diseases.[5] Subsequently, sensitive and on-site detection of Hg^{2+} in aqueous media is crucial and essential in environmental and food monitoring. Currently, the common analytical methods for mental ions detection are based on spectroscopic techniques such as atomic absorption, emission, and mass spectroscopies.[6] However, such methods are costly, labor-intensive and time-consuming, that are not suitable for on-site analyses.

A self-powered sensor for point-of-care texting is promising to be the most desirable prototype of future monitoring or detecting systems for public health and environmental protection.[7] Portable power sources with small size and light-weight design, have gained a great deal of attention in recent years due to rapid increase of power-consuming products.[8] As a new kind of green energy-conversion technology, biofuel cells (BFCs) extract bio-energy from biochemical reactions to produce electricity and exhibit many advantages in moderate conditions such as mild media and ambient temperatures.[9] In this work, a self-powered sensor for Hg^{2+} detection based on BFCs was built up. To demonstrate

the successful combination of BFC with the hollow channel μ-PADs, a novel three-dimensional microfluidic origami-based BFC analytical device (3D-μ-OBFCAD) was designed and fabricated using wax as the paper hydrophobization and insulation agent by a scalable and economical fabrication method.

DNA–metal base pairs have currently received considerable interest because of their potential applications in sensing and molecular nanoarchitectures.[10] In order to achieve high sensitivity, selectivity and simplicity detection toward Hg^{2+}, the novel approach for Hg^{2+} detection based on DNA–metal coordination chemistry[11] becomes gradually attractive. Hg^{2+} is found to specifically interact with the thymine–thymine (T-T) mismatch in DNA duplexes to form T-Hg^{2+}-T complex,[12] Herein, a mediator-less and compartment-less glucose/O_2 BFC was introduced into the hollow channels μ-PADs to implement self-powered, sensitive, and low-cost Hg^{2+} detection based on the regulation of the BFC performance caused by Hg^{2+} and T base in aptamer forming T-Hg^{2+}-T pairs for the first time.

In the 3D-μ-OBFCAD, the anode was used as the substrate for capture aptamer immobilization as well as the platform for subsequent detection. A novel porous Au-paper anodic electrode (PAE), fabricated through the growth of the Au NPs layer on the surfaces of cellulose fibers in PAE, was used for element recognition as well as conductivity enhancement. The effective electrical communication of redox enzymes with electrodes could produce high current outputs even at low concentration of the substrates, improving the sensitivity of the proposed 3D-μ-OBFCAD. Such enhanced sensitivity was also obtained by using {S2-AuNPs-GDH} bioconjugates, which featured signal aptamer (S2) and glucose dehydrogenase (GDH) labels linked to AuNPs for signal amplification. By such manner, not only the merits of high surface reactivity, good electroconductibility, and excellent biocompatibility was possessed,[13] but also the catalytic performance of GDH towards nicotinamide adenine dinucleotide (NAD^+/NADH) used as the cofactor was enhanced in this 3D-μ-OBFCAD.

In cathode, design of highly active catalysts for oxygen reduction reaction (ORR) in BFC is one of the great challenges in the field of electrochemical energy conversion.[14] The slow rate of oxygen reduction reaction (ORR) causes a large over-potential.[15] Therefore, development of highly active cathode electrocatalysts is essential. Currently, platinum (Pt) is one of the most effective electrocatalyst in BFC due to its sufficient reactivity and in bonding hydrogen and oxygen intermediates and effective catalysis in electrode reactions to form the final products.[16] To achieve high activity towards ORR, a uniform dispersion and control over the particle size of PtNPs is significant.[17] In this work, a simple synthetic route was reported to create Pt-covered carbon nanotubes (CNT/Pt) as promising nanostructured catalysts for ORR in BFC. The obtained CNT/Pt-paper cathodic electrode (PCE) not only exhibited excellent electrical conductivity favorable for catalyst toward O_2 reduction, but also avoided the instability or the deactivation of enzyme.

In this work, we described a self-powered sensor integrated with hollow channel based μ-PADs that was simple to fabricate, do not require a pump for operation, and that enable rapid fluid flow for the detection of metal ion based on oligonucleotide recognition with a mediator-less and compartment-less glucose/O_2 biofuel cell as the core component. AuNPs and CNT/Pt were employed to modify the anode and cathode which exhibited improved electric conductivity, electrochemical capability, and compatibility of the BFC device. Under optimal conditions, the proposed self-powered sensor showed wide detection range and low detection limit which demonstrated good sensitivity of the fabricated 3D-μ-OBFCAD. Additionally, the self-powered sensor also exhibited good stability and reproducibility, promising the practical application of real samples. The results demonstrated that the developed 3D-μ-OBFCAD supplied a convenient, low-cost, and sensitive method for metal ion determination. Moreover, this strategy offers a step toward the goal of conducting quantitative point-of-care assays without using auxiliary instruments or electronics.

Experimental

Materials and methods

Glucose dehydrogenase (GDH) from Thermoplasma acidophilum (E.C.1.1.1.47, 183 $U \cdot mg^{-1}$), NAD^+/NADH, ethanolamine, tetrachloroauric acid ($HAuCl_4 \cdot 4H_2O$), chloroplatinic acid ($H_2PtCl_6 \cdot 6H_2O$) and poly(dimethyldiallylammonium chloride) (PDDA) (20%, w/w in water, molecular weight = 200000−350000) were purchased from Sigma. Carbon nanotubes (CNTs) were purchased from Shenzhen Nanotech. Port. Co. Ltd. (Shenzhen, China) without further purification. Glucose was obtained from Beijing Chemical Reagent Company (Beijing, China). Whatman chromatography paper # 1 (pure cellulose paper) was purchased from GE Healthcare World-wide (Pudong Shanghai, China). The DNA oligonucleotide sequences shown below were purchased from Shanghai Linc-Bio Science Co. LTD (Shanghai, China).

Capture aptamer (S1): 5'-NH_2-(CH2)6-CAGTTTGGAC-3'

Signal aptamer (S2): 5'-NH_2-GTCCTTTCTG-3'

Ultrapure water obtained from a Millipore water purification system (≥18 MU, Milli-Q, Millipore) was used in all assays and solutions. Potassium ferricyanide, $NaBH_4$, and sodium citrate were products from Shanghai Chemical Reagent Co. All other reagents were of analytical grade and used as received.

Design and fabrication of the 3D-μ-OBFCAD

The 3D-μ-OBFCAD was comprised of four layers of patterned square papers with the same size (15.0 mm×15.0 mm), named as anodic tab (the green area), hollow channel tab (the blue area), wax channel tab (the red area) and cathodic tab (the purple area). Wax was used as the paper hydrophobization and insulation agent to construct hydrophobic barrier on paper. The microfluidic origami electronic device consisted of three unprinted line defined as folding line due to the difference of flexibility between the printed and unprinted area after baking. Then the wax-printed paper sheet was baked at 130 ℃ for 150 s to let the printed wax melt and penetrate through the paper to form the hydrophobic patterns. According to previous work, the light yellow channel was designed as half hydrophilic after baking.[4a] After cooling to room temperature, the disk-like carbon electrodes (4.0 mm in diameter) were screen-printed onto the hydrophilic zone on anodic tab and cathodic tab, respectively (Scheme 1).

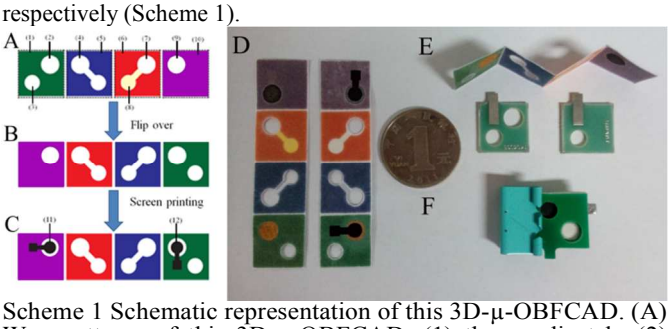

Scheme 1 Schematic representation of this 3D-μ-OBFCAD. (A) Wax patterns of this 3D-μ-OBFCAD: (1) the anodic tab; (2) hydrophilic zone for screen-printed arbon electrode; (3) inlet; (4)

hollow channel; (5) hollow channel tab; (6) 60% wax channel tab; (7) hollow reservoir; (8) 60% wax channel; (9) cathodic tab; (10) hydrophilic zone for screen-printed arbon electrode; (B) the reverse side of 3D-μ-OBFCAD; (C) pictures of the 3D-μ-OBFCAD after the screen-printing of carbon electrodes: (11) PCE; (12) PAE; (D) picture of this 3D-μ-OBFCAD; (E) picture of the folded 3D-μ-OBFCAD and the conductive connector; (F) the folded 3D-μ-OBFCAD was clamped by a home-made device folder.

The screen-printed carbon electrode together with its corresponding hydrophilic zone was denoted as "paper anodic/cathodic electrode (PAE/PCE)''. At last, the hollow channels and reservoirs were cut using, respectively, a razor blade and a 4 mm inner-diameter punch.

Synthesis of PtNPs and CNT/Pt

For the preparation of PtNPs, 4 mL H_2PtCl_6 (5%) was added to 340 mL ultrapure water and heated to 80 ℃ under stirring, followed by adding 60 mL sodium hydrogen citrate (1%) for another 1h. After that, 1 mL methanol was added and kept reflux for an additional 30 min, and then the solution changed color from pale-yellow to brown. After cooling, the synthesized PtNPs was centrifuged and dispersed in ultrapure water for further use.

The detail preparation of CNT/Pt was described as below. CNT was first carboxylate activated. Then 0.5 mg/mL of the carboxylated CNTs was dispersed into a 0.20 % PDDA aqueous solution containing 0.5 M NaCl by 30 min sonication to give a homogeneous black suspension. Residual PDDA polymer was removed by high-speed centrifugation, and the complex was thrice washed with ultrapure water to obtain PDDA-functionalized CNT. Then, the PDDA-functionalized CNT (0.75 mg) were dispersed in 9.0 mL of as-prepared colloidal PtNPs and stirred for 20 min. After centrifugation, CNT/Pt composites were obtained, which were further washed with water and redispersed in deionized water prior to use.

Preparation of AuNPs and {S2-AuNPs-GDH} bioconjugate

The AuNPs (13 nm) were synthesized by the reduction of gold ions with sodium citrate.[18] In the preparations, all the glassware was cleaned in aquaregia (HCl/HNO_3=3:1), rinsed with ultrapure water three time, and oven-dried prior to use. $HAuCl_4$ (100 mL, 0.01 %) was heated to boiling under vigorous stirring, and trisodium citrate (1.5 mL, 1 %) was added with stirring. The solution turned blue within 25 s and the final color change to red/violet occurred 70 s later. Heating to boiling was continued for an additional 10 min, the heating source was removed, and the colloid was stirred for another 15 min. The solution was allowed to cool to room temperature. The obtained AuNPs were stored at 4 ℃ prior to use.

To obtain the {S2-AuNPs-GDH} bioconjugates, 1.0 mL concentrated AuNPs mixed with GDH (10 mg·mL^{-1}, 100 μL) by sonication for 10 min. After washing with PBS (pH 7.0) and centrifugal separated, the GDH functionalized AuNPs (AuNPs-GDH) were obtained. The formed AuNPs-GDH composites were immediately redispersed into 500 μL 20 μM S2 solution respectively. The obtained mixture was incubated at room temperature with gentle mixing for 2 h. The solution was centrifuged for 15 min at 15 000 rpm, and the supernatant was removed. Followed by washing with PBS (0.01 M, pH 7.0) for further purification and separated as above. The resulting {S2-AuNPs-GDH} bioconjugates were redispersed in PBS, and were stored at 4 ℃ prior to use.

Fabrication of the self-powered Hg^{2+} sensor

As shown in Scheme 2, the porous Au-PAE was fabricated through growth of an AuNPs layer on the surfaces of cellulose fibers in the hydrophilic zone of PAE to enhance the conductivity and enlarge the effective surface area of bare PAE according to our previous work.[19] The CNT/Pt modified PCE (CNT/Pt-PCE) was obtained through assembling prepared CNT/Pt onto the surfaces of interwoven cellulose fibers in hydrophilic zone of PCE. Briefly, 10 μL prepared CNT/Pt solution was dropped into the bare hydrophilic zone in the cathodic tab and kept it for 10 min. The positively charged CNT/Pt could be tightly connect to the negative charged hydroxyl on the surface of fibers. After the dropping step, the hydrophilic zone was rinsed thoroughly according to the method demonstrated in our previous work.[20] After drying at room temperature, the CNT/Pt-PCE was obtained.

The 3D-μ-OBFCAD was constructed by immobilizing the S1 into the porous Au-PAE through the interaction between amino of S1 and Au, and incubated at room temperature for 150 s. Subsequently, unbounded S1 was washed out with PBS containing 0.05 v/v Tween-20. And 10 μL ethanolamine (1 M) was added and incubated for 150 s at room temperature to quench the remaining active groups. After washing with PBS containing 0.05 v/v Tween-20. At the same time, the {S2-AuNPs-GDH} bioconjugates was added to the conjugated area beforehand that was beneficial to develop an integrated device. Then the obtained 3D-μ-OBFCAD was stored at 4 ℃ before use.

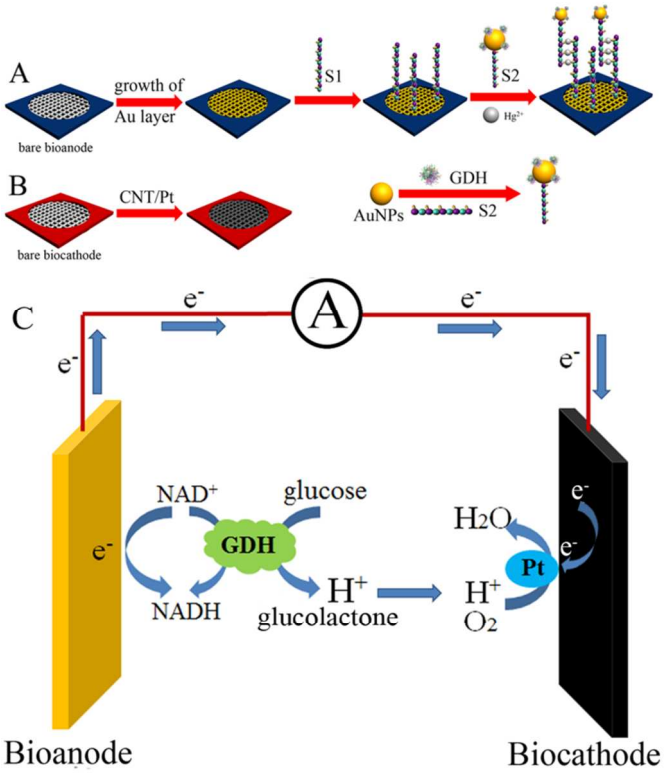

Scheme 2 Schematic diagram of the fabrication of the anode (A) and the cathode (B) in 3D-μ-OBFCAD; working mechanism of the proposed 3D-μ-OBFCAD (C).

Assay procedures of this 3D-μ-OBFCAD

The detailed procedure of Hg^{2+} detection on the proposed 3D-μ-OBFCAD is described below. 20 μL {S2-AuNPs-GDH} solutions with different concentration of Hg^{2+} was added to the modified Au-PAE and incubated for 150 s, followed by washing with washing buffer. After that, this 3D-μ-OBFCAD was immediately folded as indicated in Scheme 1E and was sequentially clamped by a home-

made device folder to ensure contact closely (Scheme 1F). Finally, 50 μL 0.1M PBS (pH 7.0) containing 10 mM NAD^+/NADH and 30 mM glucose was added into to the inlet of the 3D-μ-OBFCAD, and the solution could be transported to Au-PAE and CNT/Pt-PCE within 1 second to initiate the reaction. The output current was recorded by the electrochemical workstation (Shanghai CH Instruments Co., China), and the concentration of Hg^{2+} could be quantified by the current intensity.

Results and discussion

Characterization of PtNPs, CNT, CNT/Pt, AuNPs and AuNPs-GDH

The dispersion status of PtNPs can be found from the transmission electron microscopy (TEM), as shown in Fig. 1A, the TEM characterization suggests that the size of the PtNPs had a uniform spherical shape and was narrowly distributed with diameters in the range of 5-6 nm. A direct evidence for the attachment of PtNPs to the CNTs surface is given by the scanning electron microscopy (SEM) tests. Compared with the bare CNT (Fig. 1B), it is observed that the SEM imaging in Fig. 1C showed that the CNTs were fully covered by PtNPs. Meanwhile the energy dispersive spectrometer (EDS) shown in Fig. 1D also demonstrated the successfully preparation of CNT/Pt. The dispersion status of AuNPs solution can be found from the TEM image in Fig. 1E, and the size was about 13.0 nm. The obtained AuNPs-GDH hybrid architecture was confirmed by UV–vis absorption spectrum as shown in Fig. 1F. The as-prepared citrate-stabilized colloidal AuNPs (curve a) appeared a strong characteristic absorption peak at 524 nm which was induced by surface plasmon resonance. The absorbance of the bare AuNPs decreased with the formation of GDH-conjugated AuNPs (curve b).

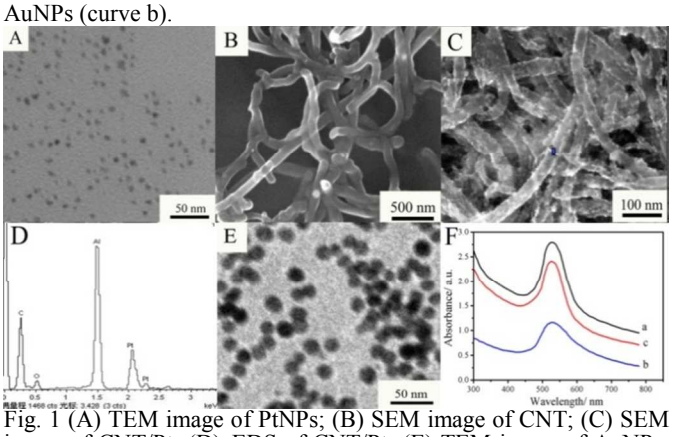

Fig. 1 (A) TEM image of PtNPs; (B) SEM image of CNT; (C) SEM image of CNT/Pt; (D) EDS of CNT/Pt; (E) TEM image of AuNPs; (F) UV-vis absorption spectrum of bare AuNPs (a), GDH-conjugated AuNPs(b), AuNPs dilution with pure water (with the same volume as GDH solution) (c).

Electrochemical characterization of the anode and cathode

Electrochemical Impedance Spectroscopy (EIS) was used for the characterization of the fabrication of the anode and cathode. As shown in Fig. 2, the bare Au-PAE showed a relatively small electron-transfer resistance, R_{et} (curve a). After the anchoring of S1 a much larger R_{et} (curve b) was obtained. Similarly, after the addition of ethanolamine and {S2-AuNPs-GDH} bioconjugates in presence of Hg^{2+} could all resist the electron-transfer kinetics of the redox probe at the Au-PAE interface, resulting in the increased impedance of the Au-PAE (curve c and d), which confirmed the immobilization of these substances. For the cathode, after CNT/Pt was formed on the cellulose fiber surface in hydrophilic zone, a much smaller R_{et} was observed (curve e). The reason may be that the CNT/Pt immobilized on the cellulose fiber surfaces played an important role similar to a conducting wire, which provided a fast electron transfer path to the paper electrode.

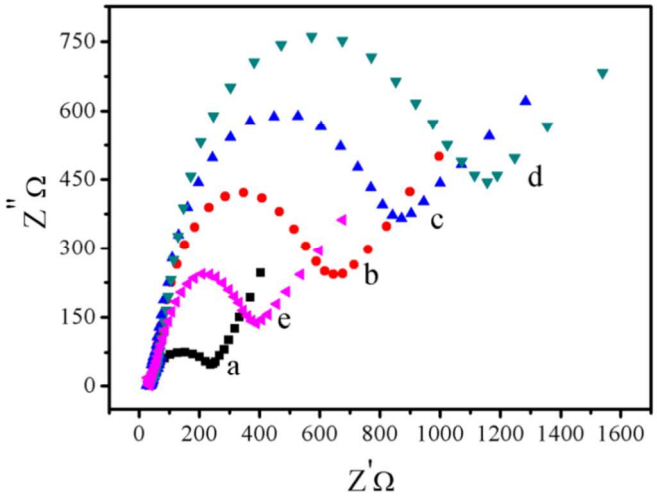

Fig. 2 (A) EIS of the anode or cathode under different condition in 10.0 mM $[Fe(CN)_6]^{3+/4+}$ solution containing 0.5 M KCl. a) Au-PAE, b) S1 modified Au-PAE, c) after the addition of ethanolamine, d) after the conjunction of {S2-AuNPs-GDH} in the presence of metal ions; e) CNT/Pt-PCE.

Electrochemical performance of the prepared porous Au-PAE and CNT/Pt-PCE

To evaluate the performance of anode, electrochemical measurements of the anode in a three-electrode cell was conducted using platinum foil as counter electrode and Ag/AgCl (saturated KCl) as reference electrode in phosphate buffer solution (PBS) (pH = 7.0) containing 10 mM NAD^+/NADH with or without 30 mM glucose. After the sandwiched aptamer reaction containing 100 nM Hg^{2+}, upon the potential scanning from -0.6 to 0.4 V, a corresponding anodic wave appeared at a low potential of -0.19 V (vs Ag/AgCl) accompanied by the oxidation of glucose as shown in Fig. 3A. Such performance was essentially identical with that for the NADH oxidation.[21] Fig. 3B showed the polarization curves of the as-prepared Au-PAE in 0.10 M PBS (pH 7.0) containing 30 mM glucose. Catalytic electrooxidation of glucose was observed at -0.2 V (vs Ag/AgCl), and the polarization current reached plateau of 570 μAcm^{-2} at -0.05 V (vs Ag/AgCl). Such prominent electrochemical catalytic property of the prepared Au-PAE toward glucose suggested that such electrode well-suited as anode for BFC.

Fig. 3C shows cyclic voltammograms (CV) of the CNT/Pt-PCE samples in N_2-saturated and O_2-saturated 0.5 M H_2SO_4 at a scan rate of 50 $mV \cdot s^{-1}$. The CV curve (Fig. 3C, curve a) in N_2-saturated H_2SO_4 (0.5 M) presented two redox peaks at around 0.35 V, which was attributed to the formation/reduction of Pt oxide and/or surface oxides on the carbon matrix.[22] While under O_2-saturated H_2SO_4 electrolyte, the curve at a voltage of over 0.55 V almost overlapped with that obtained with N_2-saturated electrolyte. But the current density at the voltage smaller than 0.55 V was significantly enhanced (Fig. 3C, curve b), indicating higher ORR activity of CNT/Pt-PCE. In Fig. 3D the ORR polarization curves of the porous Pt-PCE started at 0.9 V. The direct electron communication was beneficial for cathode development with a high potential output because of a low overpotential involved in

O_2 reduction. And such results suggested that the CNT/Pt could be used as cathode catalyst in BFC for oxygen reduction.

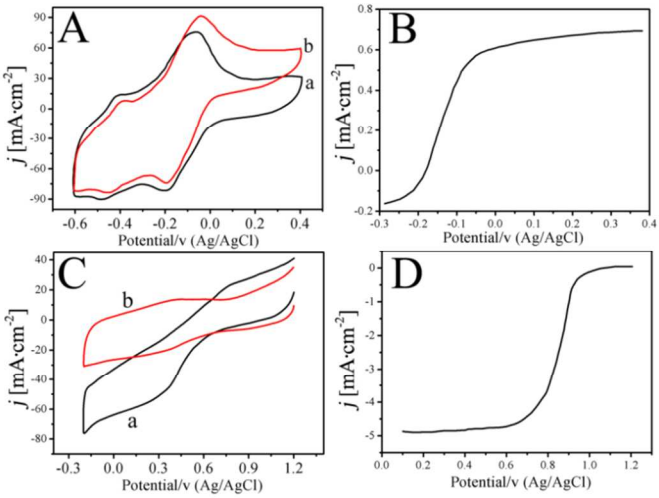

Fig. 3 (A) CV of the modified anode in 0.10 M PBS (pH 7.0) containing 0 mM (a) and 30 mM glucose (b) and 10 mM NAD^+/NADH; (B) polarization curves of the modified anode in 0.10 M PBS (pH 7.0) containing 10 mM NAD^+/NADH in the presence of 30 mM glucose; (C) CVs of the cathode in air-saturated (a) and N_2-saturated (b) 0.5 M H_2SO_4; (D) polarization curves of the cathode in air-saturated 0.5 M H_2SO_4.

Optimization of experimetal conditions

For paper-based point-of-care testing, the analytical cost, sensitivity and time efficiency is very important. The optimization procedures were performed at room temperature and consistent to the assay procedures. The effects on this 3D-μ-OBFCAD were investigated as follows. The incubation time was an important parameter to the improvement of assay efficiency, therefore to obtain the optimization reaction time, the effects of incubation time on the hybridization reaction was investigated as shown in Fig. 4A. The incubation time of the 3D-μ-OBFCAD to Hg^{2+} detection reached a maximum current intensity at 150 s, indicating the maximum formation of the sandwich aptamer reaction. Thus, an incubation time of 150 s was selected in the further study. In this work, the glucose was used as the fuel oxidized by GDH, and the concentration of glucose could influence the current intensity. Thus, the generated current was optimized by changing the concentration of glucose. As shown in Fig. 4B, when the concentration of glucose was lower than 30 mM, the current increased with increasing glucose concentration; when the concentration of glucose was higher than 30 mM, the current intensity did not increase obviously. Therefore, 30 mM glucose was used in this work.

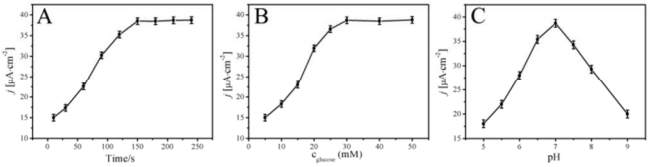

Fig. 4 (A) The effect of incubation time on current intensity at 100 nM Hg^{2+} (a) and 100 nM Ag^+ (b); (B) Effect of glucose concentration on current intensity; (C) Effect of pH value on current intensity.

To achieve an optimal current signal, the pH value of the substrate solution was the important factor to the current intensity of this 3D-μ-OBFCAD. The current intensity was measured from 5.0 to 9.0 containing 100 nM Hg^{2+}, and the maximum was observed at pH 7.0 (shown in Fig. 4C). The reason was that the high acidic or alkaline surroundings would damage the DNA molecule.[23] Since the optimal pH value for the biological systems was 7.0, the detection of this 3D-μ-OBFCAD was performed in pH 7.0 PBS containing 10 mM NADH/NAD^+ and 30 mM glucose.

Analytical performance

The working mechanism of the resulting mediator-less and compartment-less glucose/air biofuel cell for the detection of Hg^{2+} can be depicted as follows. Glucose is oxidized at anode to produce gluconolactone in the presence of GDH, and the NAD^+, NADH oxidation product, is reduced into NADH. Meanwhile, the regeneration process of NAD^+ is also smoothly completed after the produced NADH release a proton and two electrons. In cathode compartment, a proton-assisted electron transfer process has happened, molecular oxygen accepts four electrons and, assisted by protons; it is reduced to water which is friendly to the environment. The mechanism of the prepared 3D-μ-OBFCAD was proposed to be described as follows:

$$\text{glucose} \xrightarrow{GDH\ \ NAD^+} \text{gluconolactone} + \text{NADH}$$

$$\text{NADH} \rightarrow NAD^+(regeneration) + H^+ + 2e^-$$

$$O_2 + 4e^- + 4H^+ \xrightarrow{\text{Pt}} 2H_2O$$

Furthermore, the current response generated from such 3D-μ-OBFCAD was directly related to the amount of the immobilized {S2-AuNPs-GDH} bioconjugates, reflecting the concentration of mental ions. For instance, a greater amount of Hg^{2+} captured in the Au-PAE led to a higher yield of electrons and therefore a higher current response (Fig. 5A). Under the optimum conditions, as shown in Fig. 5B, the current intensity increased linearly with the logarithmic concentration of Hg^{2+} (0.1 nM – 5μM) with the calibration curve I=12.79+12.76lgcHg^{2+} (cHg^{2+}/nM) (R=0.9965). And the detection limit for Hg^{2+} was 56 pM at a signal-to-noise ratio of 3. The result demonstrated the proposed method was satisfactory for the ultrasensitive determination of Hg^{2+}. Furthermore, power curve of the assembled glucose/O_2 BFC device was investigated. Using Hg^{2+} as a model, the open-circuit voltage of the proposed 3D-μ-OBFCAD was 0.85 V and the maximum power density was 146.7 μW·cm^{-2} in the presence of 100 nM Hg^{2+} (shown in Fig. 5C).

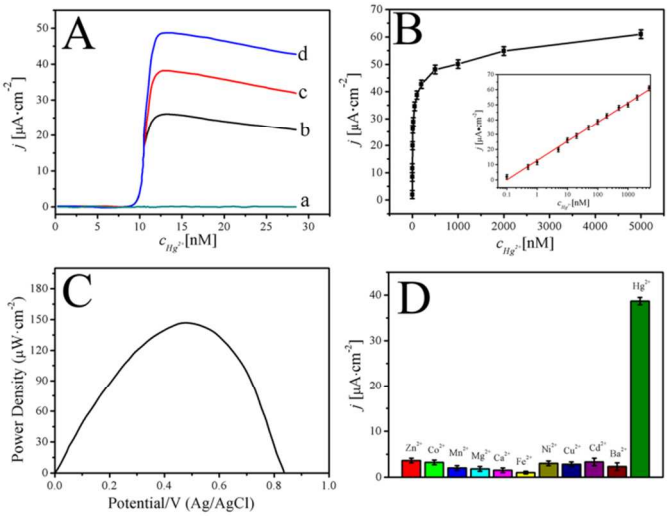

Fig. 5 (A) Current response of the 3D-μ-OBFCAD in the presence of 0, 10 nM, 100 nM and 500 nM Hg^{2+}; (B) logarithmic calibration curves for Hg^{2+} (ten measurements for each point); (C) dependence of the power density on the cell voltage in 0.10 M air saturated PBS (pH 7.0) containing 10 mM

NAD^+/NADH and 30 mM glucose; (D) Selectivity of this 3D-μ-OBFCAD to Hg^{2+}.

Additionally, the long-term storage stability of the proposed 3D-μ-OBFCAD was investigated. The proposed 3D-μ-OBFCAD stored at 4℃ for 30 days showed that the current intensity for the detection of 100 nM Hg^{2+} was 97.3% of the initial response. The average decrease in the value of the current intensity was less than 6.5% that of the freshly prepared 3D-μ-OBFCAD, when the resulting 3D-μ-OBFCAD were stored for 1 month. Consequently, the proposed 3D-μ-OBFCAD system possessed perfect stability for practical applications.

The reproducibility of this 3D-μ-OBFCAD was investigated by using the variation coefficients (CVs) of intra- and inter-assays. The intra-assay precision of the analytical method was evaluated by analyzing three concentration levels, five times per run. The CVs of the intra-assay were 4.6, 5.3 and 4.9% for 5, 10, and 50 nM Hg^{2+}, respectively. When using different batches of 3D-μ-OBFCAD, the CVs were investigated under the same conditions, and the results were 7.3, 7.6 and 6.9%. Thus, the precision and reproducibility of the 3D-μ-OBFCAD were acceptable.

In terms of the specificity, various competing metal ions were conducted for sensor performance observation, such as Zn^{2+}, Co^{2+}, Mn^{2+}, Mg^{2+}, Ca^{2+}, Fe^{2+}, Ni^{2+}, Cu^{2+}, Cd^{2+} and Ba^{2+} at 100 nM for Hg^{2+} (shown in Fig. 5D). Among various metal ions studied, Hg^{2+} performed the highest signal response against other metal ions, evidencing the high specificity and excellent selectivity of developed 3D-μ-OBFCAD for Hg^{2+} detection against other metal ions. Such good performance was due to the highly specific interaction of the T-Hg^{2+}-T coordination chemistry.

The feasibility of the method for Hg^{2+} detection using this 3D-μ-OBFCAD was evaluated in water samples from the Yellow River, a realistically complex sample containing a variety of interferences. And the results are summarized in Table 1. The good recovery (97.0-103.0% for Hg^{2+}) which indicated that the proposed system allowed the accurate quantification of Hg^{2+} in real samples without any interference from other potentially coexisting metal ions.

Table 1 Application of Hg^{2+} in real samples.

Sample	Added (nM)	Founded* ±S.D. (nM)	RSD (%)	Recovery (%)
1	5	5.03±0.13	2.31	100.6
2	10	9.97±0.15	1.96	99.7
3	50	51.46±0.43	2.30	102.9
4	100	97.63±0.57	1.84	97.63
5	500	506.51±2.34	2.16	101.3

*Average of eleven measurements.

Conclusions

In this work, a user-friendly, low-cost, integrated and self-powered sensor for Hg^{2+} detection was presented based on the regulation of the BFC performance on hollow channel μ-PADs. The capture aptamer were immobilized onto the porous Au-PAE as recognition elements. And the prepared CNT/Pt-PCE exhibited excellent electrocatalyst toward O_2 with the instability or the deactivation of enzyme avoided. Possessing the advantages of convenient, highly sensitive and cost-effective, such method was highly promising potential to be applied for sample separation and determination in public health and environmental monitoring through utilization of different recognition elements, such as molecularly imprinted polymers, antibody, and nucleic acid. Furthermore, such work also showed its great prospect in the logic gate operation which offers a step toward the goal of conducting quantitative point-of-care assays without using auxiliary instruments or electronics, and provides a new approach for self-powered nanotechnology that harvests electricity from the environment for wide applications such as implantable biomedical devices, wireless sensors, and even portable electronics.

Acknowledgements

This work was financially supported by National Natural Science Foundation of China (21475052, 21175058, 51273084); and the Natural Science Foundation of Shandong Province, China (ZR2012BZ002).

Notes and references

[a] Shandong Provincial Key Laboratory of Preparation and Measurement of Building Materials, University of Jinan, Jinan 250022, P. R. China
[b] Key Laboratory of Chemical Sensing & Analysis in Universities of Shandong, School of Chemistry and Chemical Engineering, University of Jinan, Jinan 250022, P. R. China
E-mail: chm526yanm@gmail.com; Fax:+86-531-82765959;
Tel:+86-531-82767161

1 A. W. Martinez, S. T. Phillips, M. J. Butte and G. M. Whitesides, *Angew. Chem. Int. Ed.*, 2007, **46**, 1318-1320.
2 (a) E. Carrilho, S. T.Phillips, S. J. Vella, A.W. Martinez, G.M. Whitesides, *Anal. Chem.*, 2009, 81, 5990-5998; (b) J. L. Delaney, C. F.Hogan, J. Tian, W. Shen, *Anal. Chem.*, 2011, **83**, 1300-1306.
3 C. Renault, X. Li, S. E. Fosdick, R. M. Crooks, *Anal. Chem.*, 2013, **85**, 7976-7979.
4 (a) C. Renault, M.J. Anderson, R. M. Crooks, *J. Am. Chem. Soc.*, 2014, **136**, 4616-4623; (b) S. E. Fosdick, M. J. Anderson, C. Renault, P. R. DeGregory, J. A. Loussaert, R. M. Crooks, *Anal. Chem.*, 2013, **86**, 3659-3666.
5 C.M. Wood, M.D. McDonald, P. Walker, M.J. Grosell, F. Barimo, R.C. Playle and P.J. Walsh, *Aquat. Toxicol.*, 2004, **70**, 137-157.
6 (a) Y. S. Hong, E. Rifkin, E. J. Bouwer, *Environ.Sci. Technol.*, 2011, **45**, 6429-6436; (b) J. L. Barriada, A. D. Tappin, E. H. Evans, E. P. Achterberg, *Trends Anal. Chem.*, 2007, **26**, 809-817.
7 M. Lee,J. Bae, J. Lee, C. S. Lee, S. Hong, Z. L. Wang, *Energy Environ. Sci.*, 2011, **4**, 3359-3363.
8 X. Wu, Y. Z. Guo, M. Y. Chen, X. D. Chen, *Electrochimica Acta*, 2013, **98**, 20-24.
9 (a) F. Gao, L. Viry, M. Maugey, P. Poulin, N. Mano, *Nat. Commun.*, 2010, **1**, 2; (b) T. Miyake, S. Yoshino, T. Yamada, K. Hata, M. Nishizawa, *J. Am. Chem. Soc.*, 2011, **133**, 5129-5134. (c) A. Zebda, C. Gondran, A. L. Goff, M. Holzinger, P. Cinquin, S. Cosnier, *Nat. Commun.*, 2011, **2**, 370.
10 G.H. Clever, C. Kaul and T. Carell, *Angew. Chem. Int. Ed.*, 2007, **46**, 6226-6236.
11 G.H. Clever, C. Kaul, T. Carell, *Angew. Chem.*, 2007, **119**, 6340-6350.
12 Y. Tanaka, H. Yamaguchi, S. Oda, Y. Kondo, C. Kojima and A. Ono, *J. Am. Chem. Soc.*, 2007, **129**, 244-245.

13 W. Xu, X. J. Xue, T. H. Li, H. Q. Zeng, X. G. Liu, *Angew. Chem. Int. Ed.*, 2009, **48**, 6849-6852.
14 (a) V. R. Stamenkovic, B. Fowler, B. S. Mun, G. F. Wang, P. N. Ross, C. A. Lucas, N. M. Markovic, *Science*, 2007, **315**, 493; (b) J. Zhang, K. Sasaki, E. Sutter, R. R. Adzic, *Science*, 2007, **315**, 220-222.
15 (a) X. Yuan, X. Zeng, H. J. Zhang, Z. F. Ma, C. Y. Wang, *J. Am. Chem. Soc.*, 2010, **132**, 1754-1755; (b) A. Morozan, B. Jousselme, S. Palacin, *Energy Environ. Sci.*, 2011, **4**, 1238-1254.
16 B. P. Vinayan, R. Nagar, S. Ramaprabhu, *J. Mater. Chem.*, 2012, **22**, 25325-25334.
17 E. F. Holby, W. Sheng, Y. Shao-Horn, D. Morgan, *Energy Environ. Sci.*, 2009, **2**, 865-871.
18 K. C. Grabar, R. G. Freeman, M. B. Hommer and M. J. Natan, Anal. Chem., 1995, **67**, 735–743.
19 Y. H. Wang, L. Ge, P. P. Wang, M. Yan, J. H. Yu and S. G. Ge, Chem. Commun., 2014, **50**, 1947-1949.
20 J. X. Yan, M. Yan, L. Ge, J. H. Yu, S. G. Ge and J. D. Huang, Chem. Commun., 2013, **49**, 1383–1385.
21 D. Wen, X. L. Xu, S. J. Dong, *Energy Environ. Sci.*, 2011, **4**, 1358-1363.
22 Z. X. Wu, Y. Y. Lv, Y. Y. Xia, P. A. Webley, D. Y. Zhao, *J. Am. Chem. Soc.*, 2012, **134**, 2236-2245.
23 R. Yuan, D. P. Tang, Y. Q. Chai, X. Zhong, Y. Liu and J. Y. Dai, Langmuir, 2004, **20**, 7240-7245.